EUROPEAN SOCIETY OF RADIOLOGY
Insights into Imaging

ORIGINAL ARTICLE

Open Access

Assessing abdominal aortic aneurysm growth using radiomic features of perivascular adipose tissue after endovascular repair

Rui Lv[1], Ge Hu[2], Shenbo Zhang[1], Zhe Zhang[1], Jin Chen[1], Kefei Wang[1], Zhiwei Wang[1]* and Zhengyu Jin[1]*

Abstract

Objectives The study aimed to investigate the relationship between the radiomic features of perivascular adipose tissue (PVAT) and abdominal aortic aneurysm (AAA) growth after endovascular aneurysm repair (EVAR).

Methods Patients with sub-renal AAA who underwent regular follow-up after EVAR between March 2014 and March 2024 were retrospectively collected. Two radiologists segmented aneurysms and PVAT. Patients were categorised into growing and non-growing groups based on volumetric changes observed in two follow-up computed tomography examinations. One hundred seven radiomic features were automatically extracted from the PVAT region. Univariable and multivariable logistic regression was performed to analyse radiomic features and clinical characteristics. Furthermore, the performance of the integrated clinico-radiological model was compared with models using only radiomic features or clinical characteristics separately.

Results A total of 79 patients (68 ± 9 years, 89% men) were enroled in this study, 19 of whom had a growing aneurysm. Compared to the non-growing group, PVAT of growing AAA showed a higher surface area to volume ratio (non-growing vs growing, 0.63 vs 0.70, $p = 0.04$), and a trend of low dependence and high dispersion manifested by texture features ($p < 0.05$). The area under the curve of the integrated clinico-radiological model was 0.78 (95% confidence intervals 0.65–0.91), with a specificity of 87%. The integrated model outperformed models using only radiomic or clinical features separately (0.78 vs 0.69 vs 0.69).

Conclusions Higher surface area to volume ratio and more heterogeneous texture presentation of PVAT were associated with aneurysm dilation after EVAR. Radiomic features of PVAT have the potential to predict AAA progression.

Zhiwei Wang and Zhengyu Jin contributed equally to this work.

*Correspondence:
Zhiwei Wang
zhiweiwang1981@sina.com
Zhengyu Jin
jinzy@pumch.cn
[1]Department of Radiology, State Key Laboratory of Complex Severe and Rare Disease, Peking Union Medical College Hospital, Chinese Academy of Medical Sciences and Peking Union Medical College, Beijing, China
[2]Theranostics and Translational Research Center, National Infrastructures for Translational Medicine, Institute of Clinical Medicine, Peking Union Medical College Hospital, Chinese Academy of Medical Sciences and Peking Union Medical College, Beijing, China

Springer Open

Lv *et al. Insights into Imaging* (2024)15:232

Page 2 of 9

Clinical relevance statement Radiomic features of PVAT are associated with AAA progression and can be an independent risk factor for aneurysm dilatation to assist clinicians in postoperative patient surveillance and management.

Key Points

- After EVAR for AAA, patients require monitoring for progression.
- PVAT surrounding growing AAA after EVAR exhibits a more heterogeneous texture.
- Integrating PVAT-related features and clinical features results in better predictive performance.

Graphical Abstract

Assessing abdominal aortic aneurysm growth using radiomic features of perivascular adipose tissue after endovascular repair
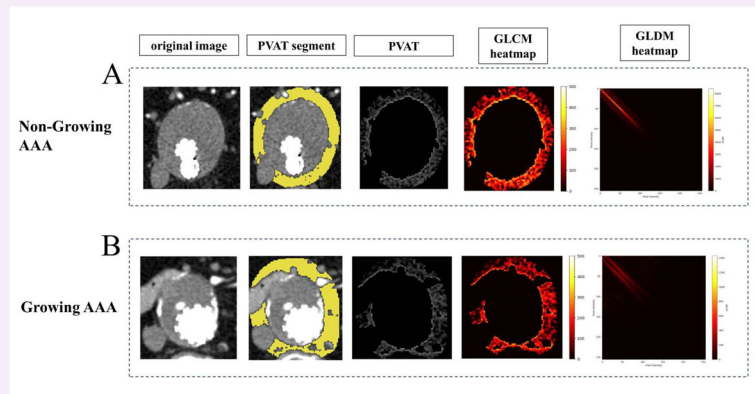
Perivascular adipose tissue surrounding a growing abdominal aortic aneurysm after endovascular aneurysm repair exhibits higher surface area-to-volume ratio and more heterogeneous texture.

Insights into Imaging

Insights Imaging (2024) Lv R, Hu G, Zhang SB, et al.
DOI: 10.1186/s13244-024-01804-7

Introduction

An abdominal aortic aneurysm (AAA) is defined as an aortic diameter of > 3 cm, with the primary risk being rupture and the associated risk of haemorrhagic death. Guidelines recommend repairing aneurysms with a maximum diameter exceeding 5.5 cm in males and 4.5 cm in females [1]. Endovascular aneurysm repair (EVAR) is a minimally invasive procedure that is safer than traditional open repair, but still requires long-term follow-up monitoring [2]. Therefore, exploring pertinent variables related to post-EVAR AAA growth is imperative for monitoring and treating AAA patients.

The causes of aneurysm growth are multifaceted, including endoleaks, endotension, hemodynamic factors, etc. Growing and non-growing groups could have factors contributing to aneurysm growth, and the level of these factors in the growing group was higher, whereas the non-growing group exhibited these factors to a lesser extent or not at all. Currently, research has shown an independent association between obesity and AAA development [3]. Perivascular adipose tissue (PVAT), which anatomically surrounds blood vessels, is now recognised as an active endocrine organ capable of secreting various adipokines, cytokines, and growth factors that can either hinder or promote the development of cardiovascular diseases [4, 5]. For aneurysms, adipose tissue infiltration into blood vessels and the secretion of proinflammatory factors may promote active macrophage infiltration, thereby inducing aneurysm development [6, 7].
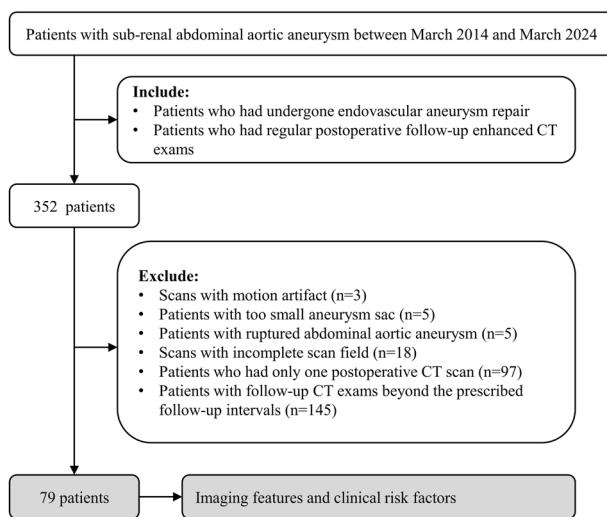
Lv *et al. Insights into Imaging* (2024)15:232

Page 3 of 9

Fig. 1 Patient selection flowchart

Additionally, research has demonstrated a correlation between PVAT and the dimensions of the thoracic and abdominal aorta, suggesting that local fat deposits may contribute to aortic remodelling [8]. Furthermore, researchers have used the radiomic features of PVAT to assess coronary artery risk, yielding results that surpass traditional risk stratification methods [9]. For AAA, increased PVAT attenuation has been independently associated with AAA growth [10], and symptomatic aneurysms exhibit higher rates of adipose tissue attenuation [11]. However, studies have not focused on differences in the radiomic features of PVAT surrounding AAAs with different growth statuses. Moreover, they have not investigated whether radiomic features can be used to predict the classification of AAA growth status. Therefore, we aimed to investigate the relationship between the radiomic features of PVAT and the status of AAA growth after EVAR and to further explore the differentiation between growing and non-growing AAAs. We hypothesised that PVAT could help predict the status of AAA progression after EVAR.

Materials and methods
Study design and population
The Institutional Review Board of Peking Union Medical College Hospital approved this retrospective study and waived the requirement for informed consent. This retrospective study included all patients with sub-renal AAAs treated at Peking Union Medical College Hospital between March 2014 and March 2024. Patients were treated with aortic-covered stent grafts from Medtronic, Inc. (Endurant, Medtronic Inc). The inclusion criteria were endovascular repair of AAAs and regular

postoperative follow-up with enhanced computed tomography (CT). The exclusion criteria included motion artefacts on scans (3 patients), small aneurysm sacs (5 patients), ruptured AAAs (5 patients), incomplete scan fields (18 patients), single follow-up CT (97 patients), and follow-up CT beyond the prescribed follow-up intervals (145 patients). The prescribed follow-up intervals were as follows: the first follow-up was scheduled 3–6 months after surgery, and the second follow-up was scheduled 9–12 months after the first follow-up. Figure 1 depicts the inclusion and exclusion criteria for patients. We retrieved clinical data from the electronic medical record system, including age, sex, history of cancer, hypertension, hyperlipidaemia, diabetes, coronary artery disease, peripheral artery disease, cerebral arteriopathy, smoking, drinking, low-density lipoprotein (LDL), high-density lipoprotein (HDL), triglycerides (TG), total cholesterol (TC), and glucose (GLU).

Image segmentation
Using the 3D Slicer software (version 5.0.3, https://www.slicer.org), two experienced radiologists, who have 5 years and 10 years of experience, respectively, manually created regions of interest (ROIs) on contrast-enhanced CT images to segment the three-dimensional AAA and calculate their volumes. The segmentation ranged from the lower renal artery level to the abdominal aorta bifurcation. We classified AAAs into growing and non-growing groups based on the volume change ratio of AAA. AAA was defined as growing if its volume increased by over 2% compared with its volume at the initial follow-up [12–15]. Subsequently, we utilised the "margin" function of the 3D Slicer software. This function grows or shrinks the selected segment by the specified margin. The segmentation of AAA was expanded outward by 10 mm [16, 17], and the original segmentation of the aneurysm was subtracted to obtain the segmentation of PVAT. The CT attenuation range was set to −195 to −45 [18, 19]. Figure 2 shows an example of the segmentation of AAA and its PVAT.

Feature extraction
The radiomic features extracted from the PVAT region included 14 shape features, 18 histogram features (also known as first-order features), and 75 texture features. The histogram features describe the statistical distribution of CT attenuation within the ROI [20]. Texture features quantify the relationships between voxel intensities and their surroundings [21], including grey-level co-occurrence matrix (GLCM) features, grey-level dependence matrix (GLDM) features, grey-level run length matrix (GLRLM) features, grey-level size zone matrix (GLSZM) features, and neighbouring grey tone difference matrix
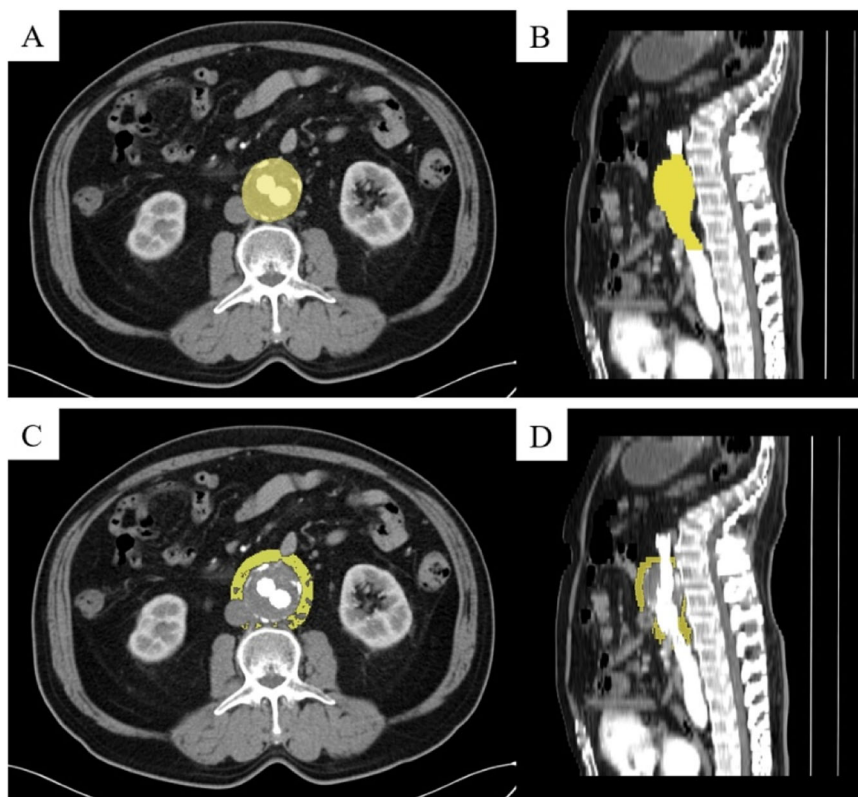
Lv *et al. Insights into Imaging* (2024)15:232

Page 4 of 9

Fig. 2 An example illustration of the segmentations of AAA and its PVAT. **A**, **B** A segmentation of AAA. **C**, **D** A segmentation of the PVAT of AAA. PVAT, perivascular adipose tissue; AAA, abdominal aortic aneurysm

(NGTDM) features. Detailed descriptions of the radiomic features can be found in supplementary materials and a separate document by Zwanenburg et al [22]. During image segmentation and feature extraction, the researchers were blinded to the patient's clinical information, including group classifications.

Statistical analysis

Statistical analyses were conducted using SPSS (version 27.0; International Business Machines Corporation). Following tests for variance homogeneity and normal distribution of variables, we conducted univariate analysis of the variables using independent samples *t*-test, nonparametric Mann–Whitney *U*-test, $\chi 2$ test, or Fisher's exact test, depending on the type of variable. To address multicollinearity among variables, we calculated the correlations between them. A correlation coefficient of > 0.8 was considered indicative of collinearity. One of the two highly correlated variables was removed, while retaining the one with the highest correlation with the dependent variable. This approach allowed us to select the most relevant independent variables for further analysis. Variables exhibiting statistically significant differences in

group comparisons were included in the binary logistic regression analysis to identify independent risk factors for AAA growth. Odds ratios (ORs) and their respective 95% confidence intervals (CIs) were determined. Receiver operating characteristic (ROC) curves were constructed to evaluate the predictive performance of the identified factors, and the area under the curve (AUC) was calculated. Differences were considered statistically significant at $p < 0.05$ (two-tailed).

Results

The agreement between the two radiologists regarding AAA growth classification was excellent (Cohen's kappa coefficient, 0.97; 95% CI: 0.75–1.19; $p < 0.001$).

Enrolment of participants

We conducted sample size estimation during the pre-experiment phase with a significance level (α) of 0.05 (two-tailed) and power (1-β) of 0.90. Consequently, a sample size of 78 patients was obtained. Between March 2014 and March 2024, 352 consecutive patients underwent endovascular repair for AAAs and regular postoperative follow-up enhanced CT. Ultimately, 79 patients

Lv *et al. Insights into Imaging* (2024)15:232

Page 5 of 9

Table 1 Demographic and clinical characteristics of participants

Variables	Overall, (*n* = 79)		*p*-value
	Non-growing AAA, (*n* = 60)	Growing AAA, (*n* = 19)	
Age, year	68 ± 8	69 ± 11	0.70
Male gender, *n* (%)	54 (90%)	16 (84%)	0.47
History of tumour, *n* (%)	10 (17%)	2 (11%)	0.72
History of hypertension, *n* (%)	38 (63%)	9 (47%)	0.22
History of hyperlipemia, *n* (%)	16 (27%)	5 (26%)	0.98
History of diabetes, *n* (%)	10 (17%)	0 (0%)	0.11
History of coronary artery disease, *n* (%)	14 (23%)	5 (26%)	0.77
History of peripheral arterial disease, *n* (%)	11 (18%)	3 (16%)	> 0.99
History of cerebral arteriopathy, *n* (%)	10 (17%)	1 (5%)	0.28
History of smoking, *n* (%)	36 (60%)	9 (47%)	0.33
History of drinking, *n* (%)	18 (30%)	4 (21%)	0.56
LDL, mmol/L	2.46 ± 0.72	3.03 ± 1.17	0.01
HDL, mmol/L	0.93 ± 0.18	1.08 ± 0.35	0.02
TG, mmol/L	1.54 ± 0.78	1.57 ± 0.85	0.89
TC, mmol/L	4.10 ± 0.82	4.87 ± 1.32	< 0.01
GLU, mmol/L	5.53 ± 1.14	5.38 ± 1.04	0.61

The data were presented as mean ± standard deviation or as numbers (percentages)

AAA abdominal aortic aneurysm, *LDL* low-density lipoprotein, *HDL* high-density lipoprotein, *TG* triglycerides, *TC* total cholesterol, *GLU* glucose

Table 2 Univariate analysis of radiomics features of PVAT among non-growing and growing AAA

Variables	Non-growing AAA	Growing AAA	*p*-value
Shape features			
Surface area to volume ratio	0.63 ± 0.14	0.70 ± 0.13	0.04
Grey-level co-occurrence matrix features			
Correlation	0.53 ± 0.07	0.50 ± 0.05	0.04
Informational measure of correlation 1	0.14 ± 0.03	0.13 ± 0.02	0.03
Inverse variance	0.46 ± 0.02	0.47 ± 0.02	0.04
Maximal correlation coefficient	0.63 ± 0.11	0.57 ± 0.08	0.04
Maximum probability	0.22 ± 0.04	0.20 ± 0.04	0.03
Grey-level dependence matrix features			
Dependence non-uniformity normalised	0.05 ± 0.01	0.06 ± 0.005	0.02
Dependence variance	29.88 ± 4.51	26.96 ± 4.13	0.01
Large dependence emphasis	141.17 ± 27.97	124.55 ± 22.08	0.02
Grey-level run length matrix features			
Long run emphasis	4.76 ± 1.00	4.20 ± 0.78	0.01
Run length non-uniformity normalised	0.50 ± 0.05	0.52 ± 0.04	0.01
Run percentage	0.64 ± 0.04	0.66 ± 0.03	0.01
Run variance	1.80 ± 0.53	1.50 ± 0.42	0.01
Short run emphasis	0.72 ± 0.04	0.74 ± 0.03	0.04

PVAT perivascular adipose tissue, *AAA* abdominal aortic aneurysm

were included in this study. Table 1 summarises the detailed demographic and clinical characteristics.

Univariate analysis among non-growing and growing AAA after EVAR

Table 1 presents the statistical data on the clinical characteristics of patients with growing or non-growing AAA after EVAR. LDL (2.46 vs 3.03, $p = 0.01$), HDL (0.93 vs 1.08, $p = 0.02$), and TC (4.10 vs 4.87, $p = 0.02$) showed significant differences between the growing or non-growing AAA groups, whereas no significant differences were found in the remaining clinical parameters.

Table 2 summarises the statistical data of the radiomics features of the PVAT surrounding growing or non-growing AAAs after EVAR. It comprises 1 shape feature and 13 texture features, including GLCM, GLDM, and GLRLM features. Significant differences between the two groups were observed, including surface area-to-volume ratio (0.63 vs 0.70, $p = 0.04$), correlation (0.53 vs 0.50, $p = 0.04$), an informational measure of correlation 1 (0.14 vs 0.13, $p = 0.03$), Inverse variance (0.46 vs 0.47, $p = 0.04$),

maximal correlation coefficient (0.63 vs 0.57, $p = 0.04$), Maximum probability (0.22 vs 0.20, $p = 0.03$), dependence non-uniformity normalised (0.05 vs 0.06, $p = 0.02$), Dependence variance (29.88 vs 26.96, $p = 0.01$), large dependence emphasis (141.17 vs 124.55, $p = 0.02$), long-run emphasis (4.76 vs 4.20, $p = 0.01$), run length non-uniformity normalised (0.50 vs 0.52, $p = 0.01$), run percentage (0.64 vs 0.66, $p = 0.01$), run variance (1.80 vs 1.50, $p = 0.01$), and short-run emphasis (0.72 vs 0.74, $p = 0.04$). Regarding histogram features, we did not find any evidence of differences between the two groups. Regarding texture features, including GLRLM, GLSZM, and NGTDM features, we also did not find statistically significant results. Table 2 shows the detailed results.

Figure 3 illustrates two examples of the texture of PVAT surrounding growing or non-growing AAAs. Comparing the GLCM texture heatmaps of PVAT, growing AAAs exhibited darker regions with lower GLCM values, whereas non-growing AAAs exhibited brighter regions with higher GLCM values. The GLDM texture heatmaps showed that growing AAAs exhibited patterns farther
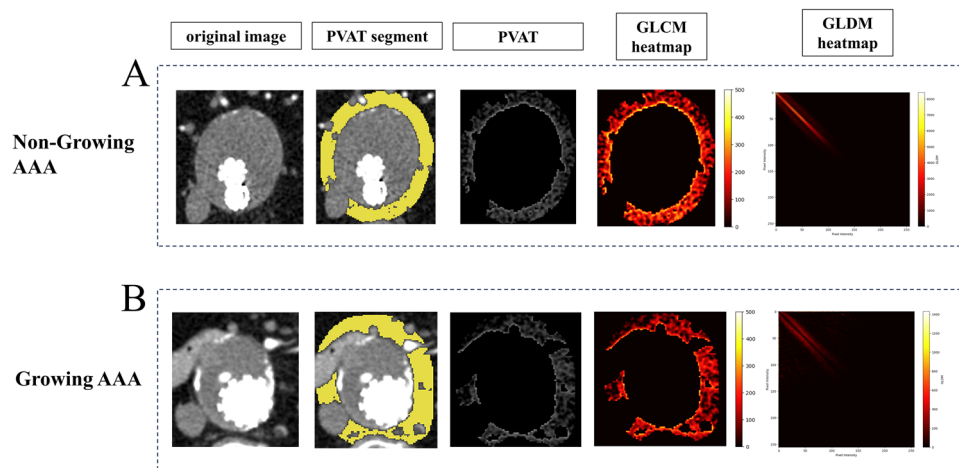
Lv *et al. Insights into Imaging* (2024)15:232

Page 6 of 9

Fig. 3 The visualisation of texture features. **A** A 68-year-old male in the non-growing AAA group. The first image in the top row displays the arterial phase enhanced CT slice of the maximum axial plane of the AAA. The second image from the top represents the manual segmentation of PVAT conducted by radiologists. The third image depicts the extracted PVAT. The fourth and fifth images display the heatmaps of the GLCM and GLDM, respectively. **B** A 74-year-old male in the growing AAA group. The image of (**B**) represents the same meaning as (**A**). AAA, abdominal aortic aneurysm; PVAT, perivascular adipose tissue; GLCM, grey level co-occurrence matrix; GLDM, grey level dependence matrix

Table 3 Evaluation of logistic regression model for AAA growth

Evaluation index	Radiomic model	Clinical model	Clinico-radiological integrated model
The p-value of omnibus test	0.01	< 0.01	< 0.01
The p-value of Hosmer–Lemeshow test	0.98	0.24	0.47
Percentage accuracy in classification (%)	75%	79%	80%
AUC (95% CI)	0.69 (0.55–0.83)	0.69 (0.54–0.84)	0.78 (0.65–0.91)
The p-value of AUC	0.02	0.02	< 0.01
Sensitivity	74%	74%	68%
Specificity	65%	65%	87%
Cutoff value	0.25	0.25	0.31

AAA abdominal aortic aneurysm, *AUC* area under curve, *CI* confidence interval

from the diagonal lines. In Fig. 3, differences in the texture of PVAT were visually observed between the two groups.

Binary logistic regression analysis among non-growing and growing AAA after EVAR

Among the 79 patients, 19 (24%) had non-growing AAA. The variables included in the binary logistic regression model were determined using univariate analysis ($p = 0.05$). The dependence variances of PVAT and TC were included in the binary logistic regression model.

The ORs for these two features are 0.84 (95% CI: 0.72–0.98, $p = 0.03$) and 2.24 (95% CI 1.20–4.17, $p = 0.01$), respectively. The AUC of this model was 0.78 (95% CI: 0.65–0.91, $p < 0.01$), with a sensitivity of 68% and specificity of 87%. Additionally, by comparing the model combining radiomic and clinical features with models using only radiomic features or clinical features

separately, their AUCs were 0.69 (95% CI: 0.55–0.83, $p = 0.02$) and 0.69 (95% CI: 0.54–0.84, $p = 0.02$), respectively. Table 3 lists the evaluation indices of the three models. All three models showed statistical significance (Omnibus test, $p < 0.01$) and had good goodness-of-fit (Hosmer–Lemeshow test, $p > 0.05$). We found that the clinico-radiological integrated model outperformed the individual models. Figure 4 shows the ROC curves of the three models.

Discussion

In this study, we analysed the radiomic features of PVAT on follow-up enhanced CT after EVAR and the clinical characteristics of patients to explore the association between PVAT and AAA growth status. The clinical-radiological integrated model achieved the best performance, with an AUC of 0.78. Our finding holds significant

Lv *et al. Insights into Imaging*   (2024)15:232
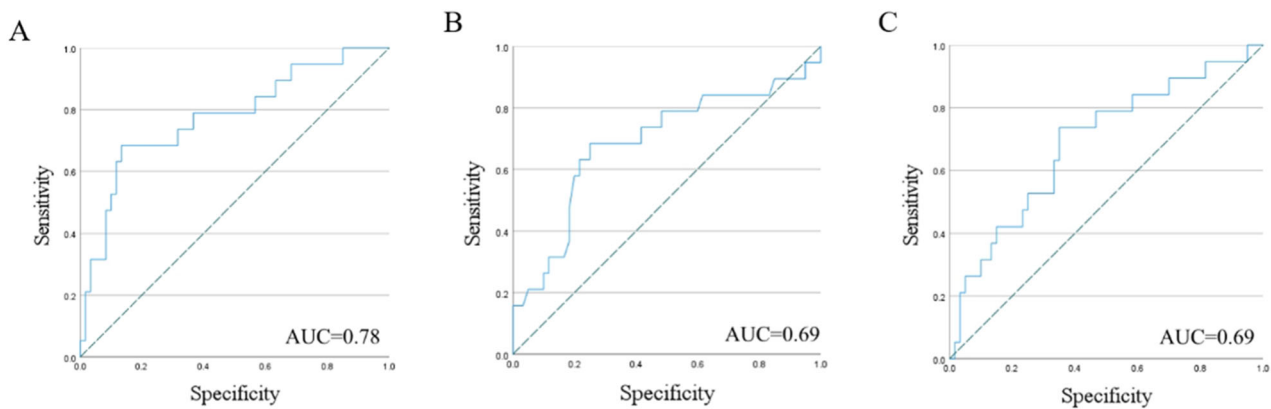
Page 7 of 9

Fig. 4 ROC curves of radiomic signature in predicting AAA growth classification in different models. **A** Clinico-radiological integrated model. **B** Radiomic model. **C** Clinical model. AAA, abdominal aortic aneurysm; AUC, area under the curve

clinical value for the long-term follow-up of patients after EVAR.

The results of the univariate analysis indicated that PVAT surrounding growing AAA after EVAR had a higher surface area-to-volume ratio, which aligns with the theory of fat adhering closely to blood vessels and potentially facilitating the infiltration or secretion of PVAT [4, 23]. Regarding texture features, previous studies have shown that texture analysis of aneurysms and thrombi can effectively predict aneurysm expansion [12, 24]. In our study, both GLCM and GLDM results indicated that PVAT surrounding growing AAA exhibited low dependence and high dispersion. The heatmaps of GLCM and GLDM for growing and non-growing AAAs illustrate texture differences between the two, suggesting that the internal composition of PVAT in growing AAAs is more heterogeneous [22]. This discovery may motivate researchers to investigate the use of PVAT texture features in classifying AAA growth.

Dependence variance describes the texture and structure of images and measures the variability of the greyscale differences between pairs of pixels across the entire image. The calculation is done using GLCM, where the variance of greyscale differences in GLCM yields dependence variance [20, 21]. Our results indicate that a lower variability in greyscale differences of PVAT, indicating more uniform greyscale differences, may correspond to a higher risk of AAA growth after EVAR. Serum TC measurement includes various types of cholesterol particles present in the blood. Studies have shown a positive correlation between serum TC levels and AAA growth [25, 26], which is consistent with previous findings.

No significant difference was found in CT attenuation between the two PVAT groups (-81.80 vs -80.06, $p = 0.28$), with a single-factor logistic analysis yielding an AUC value of 0.596 (95% CI: 0.448–0.744, $p = 0.21$),

which was significantly lower than that of the other models in this study. This may benefit future research in identifying the relevant features for predicting AAA expansion, especially in post-EVAR studies.

Long-term follow-up is required to monitor evolutions after EVAR [2]. Some researchers have focused on monitoring postoperative complications, such as persistent type 2 endoleaks, and radiomics features have been used to establish machine learning algorithms for predicting aggressive type 2 endoleaks after EVAR [27]. Researchers have also developed radiomics models for AAA to predict the outcomes of various postoperative complications after EVAR [28, 29]. Rapid growth in volume or diameter typically indicates unfavourable evolution, and monitoring these parameters may facilitate the early detection of AAA evolutions. For instance, efforts have been made to identify the post-EVAR shrinkage of AAA [30] or to classify post-EVAR AAA evolutions using radiomics texture analysis [31]. This study monitored changes in AAA volume and demonstrated that differences in PVAT may lead to variations in AAA volume.

PVAT has been extensively studied for its pathophysiological effects on blood vessels [4, 23, 32]. Due to its significant impact on blood vessels, researchers have attempted to integrate PVAT with traditional predictive features in previous studies. For example, adding PVAT radiomics to the CT-derived fractional flow reserve model enhanced the diagnostic performance for detecting haemodynamically significant coronary artery stenosis [33]. Extracting the radiomics features of PVAT and carotid plaques improved the model's capability to identify symptomatic carotid plaques [34]. Current research on PVAT of AAA has often focused on the attenuation of adipose tissue around the aorta [10, 16, 35], highlighting its association with AAA growth. Additionally, studies have shown that PVAT density around the aneurysm sac

Lv *et al. Insights into Imaging* (2024)15:232

Page 8 of 9

exceeds that in healthy vessels [11]. Our study expands the scope of the application of PVAT in predicting AAA growth by demonstrating the relationship between the radiomics features of PVAT and post-EVAR AAA evolution. Integrating these features into predictive models, alongside traditional clinical features, improves the model's predictive performance. Multivariate Cox regression analysis revealed that the baseline maximum diameter and high PVAT attenuation were independent predictors of AAA progression [10]. Furthermore, one study found that the average CT attenuation of PVAT predicted AAA growth with an AUC of 0.688, which increased to 0.797 when combined with the baseline AAA diameter [16]. Our model demonstrated a similar performance to theirs. Furthermore, the model achieved a specificity of 87%, indicating its ability to effectively exclude false positives and minimise the misclassification of non-growing AAA cases as growth cases. In future research, we plan to establish a comprehensive model that incorporates the aneurysm sac, intraluminal thrombus, clinical features, and PVAT to evaluate the predictive value of PVAT and the predictive ability of the model.

This study has several limitations. Due to the need for relatively stable conclusions, strict follow-up intervals were set, resulting in a smaller final sample size. We calculated the estimated sample size for the overall study in the pre-experiment to minimise the impact of the small sample size. In the future, we will increase the sample size to further explore the relationship between PVAT and AAA. This retrospective study highlighted the necessity for prospective and long-term follow-up studies. There were also limitations related to the development of image segmentation techniques, necessitating manual intervention for three-dimensional aneurysm segmentation. Currently, complete automation through software programmes remains unattainable.

In conclusion, the PVAT of growing AAA after EVAR exhibits a higher surface area-to-volume ratio and more heterogeneous texture. The radiomic features of PVAT exhibit significant differences between patients with growing or non-growing AAA and can help categorise the AAA growth status after EVAR with high specificity. Integrating PVAT-related features into predictive models alongside traditional clinical features can improve the model's predictive performance.

Abbreviations

AAA	Abdominal aortic aneurysm
AUC	Area under curve
CI	Confidence interval
CT	Computed tomography
EVAR	Endovascular aneurysm repair
GLCM	Grey-level co-occurrence matrix
GLDM	Grey-level dependence matrix
GLRLM	Grey-level run length matrix
GLSZM	Grey-level size zone matrix
GLU	Glucose
HDL	High-density lipoprotein
LDL	Low-density lipoprotein
NGTDM	Neighbouring grey tone difference matrix
OR	Odds ratio
PVAT	Perivascular adipose tissue
ROC	Receiver operating characteristic
ROI	Region of interest
TC	Total cholesterol
TG	Triglycerides

Supplementary information

The online version contains supplementary material available at https://doi.org/10.1186/s13244-024-01804-7.

ELECTRONIC SUPPLEMENTARY MATERIAL

Declarations

Ethics approval and consent to participate

Institutional Review Board approval was obtained. This study was approved by the institutional review board of Peking Union Medical College Hospital.

Consent for publication

Not applicable.

Competing interests

The authors declare that they have no competing interests.

References

1. Schanzer A, Oderich GS (2021) Management of abdominal aortic aneurysms. N Engl J Med 385:1690–1698
2. Wanhainen A, Verzini F, Van Herzeele I et al (2019) Editor's choice—European Society for Vascular Surgery (ESVS) 2019 clinical practice guidelines on the management of abdominal aorto-iliac artery aneurysms. Eur J Vasc Endovasc Surg 57:8–93
3. Eckstein H-H, Maegdefessel L (2020) Linking obesity with abdominal aortic aneurysm development. Eur Heart J 41:2469–2471
4. Villacorta L, Chang L (2015) The role of perivascular adipose tissue in vasoconstriction, arterial stiffness, and aneurysm. Horm Mol Biol Clin Investig 21:137–147
5. Iozzo P (2011) Myocardial, perivascular, and epicardial fat. Diabetes Care 34:S371–S379

Lv *et al. Insights into Imaging* (2024)15:232

Page 9 of 9

6. Henrichot E, Juge-Aubry CE, Pernin AS et al (2005) Production of chemokines by perivascular adipose tissue. Arterioscler Thromb Vasc Biol 25:2594–2599

7. Blomkalns AL, Gavrila D, Thomas M et al (2013) CD14 directs adventitial macrophage precursor recruitment: role in early abdominal aortic aneurysm formation. J Am Heart Assoc 2:e000065

8. Thanassoulis G, Massaro JM, Corsini E et al (2012) Periaortic adipose tissue and aortic dimensions in the Framingham heart study. J Am Heart Assoc 1:e000885

9. Oikonomou EK, Williams MC, Kotanidis CP et al (2019) A novel machine learning-derived radiotranscriptomic signature of perivascular fat improves cardiac risk prediction using coronary CT angiography. Eur Heart J 40:3529–3543

10. Zhang S, Gu H, Chang N et al (2023) Assessing abdominal aortic aneurysm progression by using perivascular adipose tissue attenuation on computed tomography angiography. Korean J Radiol 24:974–982

11. Dias-Neto M, Meekel JP, van Schaik TG et al (2018) High density of periaortic adipose tissue in abdominal aortic aneurysm. Eur J Vasc Endovasc Surg 56:663–671

12. Ding N, Hao Y, Wang Z et al (2020) CT texture analysis predicts abdominal aortic aneurysm post-endovascular aortic aneurysm repair progression. Sci Rep 10:12268

13. Hu G, Ding N, Wang Z, Jin Z (2022) The association of body composition with abdominal aortic aneurysm growth after endovascular aneurysm repair. Insights Imaging 13:76

14. Bley TA, Chase PJ, Reeder SB et al (2009) Endovascular abdominal aortic aneurysm repair: nonenhanced volumetric CT for follow-up. Radiology 253:253–262

15. Demehri S, Signorelli J, Kumamaru KK, Wake N, Rybicki FJ (2015) Volumetric quantification of type II endoleaks: an indicator for aneurysm sac growth following endovascular abdominal aortic aneurysm repair. Radiology 271:282–290

16. Yamaguchi M, Yonetsu T, Hoshino M et al (2021) Clinical significance of increased computed tomography attenuation of perivascular adipose tissue in patients with abdominal aortic aneurysms. Circ J 85:2172–2180

17. Lapid B, Wu H, Weintraub N (2024) Indicators of increased CT attenuation of perivascular adipose tissue in abdominal aortic aneurysms. J Cardiovasc Comput Tomogr 18:S36–S36

18. Schlett CL, Massaro JM, Lehman SJ et al (2009) Novel measurements of periaortic adipose tissue in comparison to anthropometric measures of obesity, and abdominal adipose tissue. Int J Obes (Lond) 33:226–232

19. Sjostrom L, Kvist H, Cederblad A, Tylen U (1986) Determination of total adipose tissue and body fat in women by computed tomography, 40K, and tritium. Am J Physiol 250:E736

20. Mayerhoefer ME, Materka A, Langs G et al (2020) Introduction to radiomics. J Nucl Med 61:488–495

21. van Griethuysen JJM, Fedorov A, Parmar C et al (2017) Computational radiomics system to decode the radiographic phenotype. Cancer Res 77:e104–e107

22. Zwanenburg A, Leger S, Vallières M, Lck S (2016) Image biomarker standardisation initiative. Radiology. https://doi.org/10.48550/arXiv.1612.07003

23. Henrichot E (2005) Production of chemokines by perivascular adipose tissue: A role in the pathogenesis of atherosclerosis? Arterioscler Thromb Vasc Biol 25:2594

24. Rezaeitaleshmahalleh M, Mu N, Lyu Z et al (2023) Radiomic-based textural analysis of intraluminal thrombus in aortic abdominal aneurysms: a demonstration of automated workflow. J Cardiovasc Transl Res 16:1123–1134

25. Deeg MA, Meijer CA, Chan LS, Shen L, Lindeman JHN (2016) Prognostic and predictive biomarkers of abdominal aortic aneurysm growth rate. Curr Med Res Opin 32:509–517

26. Nana P, Dakis K, Brodis A, Spanos K, Kouvelos G (2021) Circulating biomarkers for the prediction of abdominal aortic aneurysm growth. J Clin Med 10:1718

27. Charalambous S, Klontzas ME, Kontopodis N et al (2021) Radiomics and machine learning to predict aggressive type 2 endoleaks after endovascular aneurysm repair: a proof of concept. Acta Radiol 63:1293–1299

28. Wang Y, Zhou M, Ding Y et al (2022) A radiomics model for predicting the outcome of endovascular abdominal aortic aneurysm repair based on machine learning. Vascular 31:654–663

29. Wang Y, Zhou M, Ding Y et al (2022) Development and comparison of multimodal models for preoperative prediction of outcomes after endovascular aneurysm repair. Front Cardiovasc Med 9:870132

30. van Rijswijk RE, Groot Jebbink E, Holewijn S, Stoop N, van Sterkenburg SM, Reijnen MMPJ (2022) Predictors of abdominal aortic aneurysm shrinkage after endovascular repair. J Clin Med 11:1394

31. García G, Maiora J, Tapia A, Blas MD (2012) Evaluation of texture for classification of abdominal aortic aneurysm after endovascular repair. J Digit Imaging 25:369–376

32. Kotanidis C, Antoniades C (2021) Perivascular fat imaging by computed tomography (CT): a virtual guide. Br J Pharmacol 178:4270–4290

33. Yu L, Chen X, Ling R et al (2022) Radiomics features of pericoronary adipose tissue improve CT-FFR performance in predicting hemodynamically significant coronary artery stenosis. Eur Radiol. https://doi.org/10.1007/s00330-022-09175-7

34. Chen C, Tang W, Chen Y et al (2023) Computed tomography angiography-based radiomics model to identify high-risk carotid plaques. Quant Imaging Med Surg 13:6089–6104

35. Debono S, Tzolos E, Syed MBJ et al (2024) CT attenuation of periaortic adipose tissue in abdominal aortic aneurysms. Radiol Cardiothorac Imaging 6:e230250

Publisher's Note